

# Kinetics of protein-release by an aptamer-based DNA nanodevice

A. Reuter, W.U. Dittmer, and F.C. Simmel<sup>a</sup>

Department of Physics and Center for Nanoscience, LMU München, Geschwister-Scholl-Platz 1, 80539 Munich, Germany

Received 26 June 2006 / Received in final form 19 January 2007

Published online: 16 February 2007 – © EDP Sciences, Società Italiana di Fisica, Springer-Verlag 2007

**Abstract.** A recently introduced DNA nanodevice can be used to selectively bind or release the protein thrombin triggered by DNA effector strands. The release process is not well described by simple first or second order reaction kinetics. Here, fluorescence resonance energy transfer and fluorescence correlation spectroscopy experiments are used to explore the kinetics of the release process in detail. To this end the influence of concentration variations and also of temperature is determined. The relevant kinetic parameters are extracted from these experiments and the kinetic behavior of the system is simulated numerically using a set of rate equations. The hydrodynamic radii of the aptamer device alone and bound to thrombin are determined as well as the dissociation constant for the aptamer device-thrombin complex. The results from the experiments and a numerical simulation support the view that the DNA effector strand first binds to the aptamer device followed by the displacement of the protein.

**PACS.** 82.35.Pq Biopolymers, biopolymerization – 82.39.Pj Nucleic acids, DNA and RNA bases – 87.15.He Dynamics and conformational changes

## 1 Introduction

DNA has been used for the construction of a variety of nanomechanical devices capable of performing simple movements (for reviews see [1,2]). In several cases these conformational changes can be induced by so-called “fuel” or “effector” strands which can be added to the device and selectively removed again in a process known as branch migration. Recently, this principle was combined with the binding properties of DNA aptamers to construct a simple molecular device which can grab or release a protein [3]. The operation of this device was monitored in electrophoretic band shift experiments and in fluorescence resonance energy transfer (FRET) experiments as well as in fluorescence anisotropy measurements. It was found that the kinetics of protein release cannot be described by a simple first or second order kinetic process alone. Several scenarios are conceivable for the protein release in which the DNA fuel strands play a more or less active role: they can either bind to the device-protein complex and actively help to displace the protein, or they can simply bind to available free aptamer devices and thereby shift the chemical equilibrium between the free and protein-bound aptamers. In order to clarify this issue, we here perform a more thorough investigation of the device kinetics. A detailed account of the reaction steps involved in the protein release by the aptamer device is given. The dissociation constant  $K_d$  of the device-protein complex is determined

by fluorescence correlation spectroscopy (FCS). The kinetics of the protein release by the aptamer device triggered by a fuel strand is then measured in FRET experiments as a function of fuel strand concentration and of temperature. Subsequently, a kinetic model is employed to describe the time course of fluorescence decay in these experiments during the release of the protein from the device. From  $K_d$ , the appropriate initial concentrations of the device and thrombin are obtained. From the kinetic model the rate-determining steps in the release process can be deduced. This identifies the relevant processes leading to the displacement of the protein from the aptamer device.

## 2 Experimental section

### 2.1 Operation principle of the aptamer device

The operation principle of the aptamer device has been described in detail in [3]. Briefly, to construct the device the sequence of an anti-thrombin aptamer (5'- GGTTG-GTGTGGTTGG -3' [4]) has been extended by a 12 base long “toehold” section (5'- TAAGTTCATCTC -3') which serves as point of attachment for a fuel strand  $F$  (5'- CACCAACCGAGATGAACTTACGGCGTTG -3').  $F$  is partly complementary to the aptamer sequence and may form a DNA duplex with the aptamer, resulting in the displacement of the protein. The reaction steps involved in protein release are schematically depicted in Figure 1.

<sup>a</sup> e-mail: [simmel@lmu.de](mailto:simmel@lmu.de)

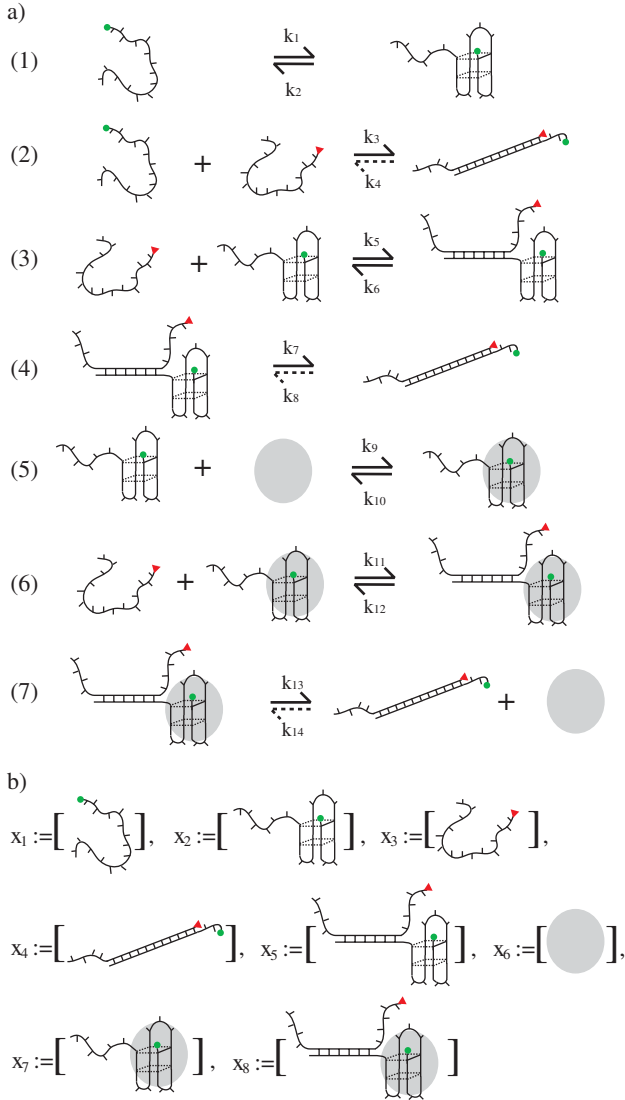


**Fig. 1.** (a) Schematic representation of reaction steps involved in the release process: in the absence of protein, the aptamer device strand may be present in a folded or in an unfolded form (1). Added fuel strands may bind to the unfolded (2) or the folded (3) device. Binding to the folded device may first occur at the unstructured “toehold” section (3) from which complete hybridization may proceed (4). In the presence of protein, the aptamer device can bind to it with dissociation constant  $K_d = k_{10}/k_9$  (5). After addition of fuel strand, now also an intermediate complex of aptamer device, protein, and fuel strand can be formed (6). Finally, displacement of the protein from the device and complete binding of fuel to device leads to the release of protein (7). (b) Definition of concentrations  $x_1, x_2, \dots, x_8$  for the kinetic model.

The fuel strand  $F$  can be removed from the aptamer by a complementary “removal” strand in a process known as branch migration. In this way, the aptamer device can be cyclically switched between a protein-binding and a non-binding form. In the present work, we are only concerned with the release process.

## 2.2 Fluorescence resonance energy transfer

For fluorescence experiments, the aptamer device strand was labeled at the 3′ end via an additional thymidine residue with the fluorophore Oregon Green 488 (OG488, Molecular Probes/Invitrogen, Karlsruhe, Germany) and the fuel strand was labeled with TAMRA (5(6)-carboxytetramethylrhodamine) at the 5′ end. FRET is the radiationless transfer of energy between two fluorophores with overlapping excitation and emission spectra. The transfer efficiency strongly depends on the separation of the two dyes and can be used to characterize molecular motion and binding events. An overview of FRET can be found in reference [5]. FRET experiments were performed on a FluoroLog-322 spectrofluorometer (Horiba Jobin-Yvon, Longjumeau, France). Fluorescence of OG488 was excited with a 450 W Xenon lamp bandpass filtered at 488 nm by a double grating and detected with a photomultiplier detector through a second grating at 518 nm. Emission and excitation slits were set to 5 nm. The content of the sample cuvette was stirred and temperature controlled by the Peltier element F3004. The concentration of the aptamer device was 1  $\mu\text{M}$  for the first and 50 nM for the second series of experiments. Thrombin was added in the specified amount (no thrombin, 1:5, 1:1, 5:1 ratio) to the aptamer device and incubated for one hour before starting the experiments. The fuel strand  $F$  was then added in stoichiometry with the aptamer. Fluorescence intensity was integrated for one second for each data point. The data was recorded using the DataMax software provided by the fluorometer manufacturer and further processed using Igor Pro (Wave Metrics, Portland, OR, USA).

## 2.3 Fluorescence correlation spectroscopy

### 2.3.1 Theory and data processing

Fluorescence correlation spectroscopy (FCS) is a statistical method for the determination of important physical parameters of fluorescently labeled species such as diffusion constants [6–12]. FCS measurements are usually performed using a confocal microscope setup (see below). If a diffusing fluorescent molecule or particle passes through the confocal detection volume, fluorescence photons are emitted that are detected and counted. The number of fluorescence photons is evaluated statistically by means of an autocorrelation analysis in order to obtain characteristic diffusion times and constants. The autocorrelation function  $G$  for an ellipsoidal detection volume with Gaussian intensity distribution is:

$$G(t) = 1 + \frac{1}{N} \cdot G_{\text{Diff}}(t, \tau_D) \quad (1)$$

$$G_{\text{Diff}}(t, \tau_D) = \frac{1}{1 + (t/\tau_D)} \cdot \frac{1}{\sqrt{1 + 1/S^2 \cdot (t/\tau_D)}} \quad (2)$$

where  $N$  denotes the average number of labeled molecules inside the detection volume,  $t$  the correlation time, and

$\tau_D$  the characteristic diffusion time which is inversely proportional to the diffusion coefficient  $D$ :

$$\tau_D = \frac{\omega_{xy}^2}{4D}. \quad (3)$$

The structure parameter  $S$  is given by

$$S = \omega_z / \omega_{xy}, \quad (4)$$

where  $\omega_{xy}$  is the radius of the detection volume parallel to the beam and  $\omega_z$  is the radius of the detection volume perpendicular to the beam [8].

For two fluorescent components with differing diffusion constants the diffusion part of the autocorrelation function  $G_{\text{Diff}}$  becomes:

$$G_{\text{Diff}}(t, \tau_{D1}, \tau_{D2}) = (1 - Y) \cdot \frac{1}{1 + (t/\tau_{D1})} \cdot \frac{1}{\sqrt{1 + 1/S^2 \cdot (t/\tau_{D1})}} + Y \cdot \frac{1}{1 + (t/\tau_{D2})} \cdot \frac{1}{\sqrt{1 + 1/S^2 \cdot (t/\tau_{D2})}} \quad (5)$$

where  $1 - Y$  denotes the fraction of molecules moving with the diffusion constant  $\tau_{D1}$  and  $Y$  the fraction with diffusion constant  $\tau_{D2}$  [12].

For the fluorescent dyes used, the formation of triplet states has to be taken into account already at the relatively low excitation intensities used. The relaxation time of the triplet state  $\tau_{\text{Tr}}$  depends on the dye and is typically on the order of a few microseconds. The autocorrelation function can thus be written [9, 12]:

$$G(t) = 1 + \frac{1}{N} \cdot G_{\text{Diff}}(t, \tau_{D1}, \tau_{D2}) \cdot G_{\text{Tr}}(t, \tau_{\text{Tr}}) \quad (6)$$

with

$$G_{\text{Tr}}(t, \tau_{\text{Tr}}) = 1 + \frac{\Theta \cdot \exp(-t/\tau_{\text{Tr}})}{1 - \Theta} \quad (7)$$

where  $\Theta$  is the triplet fraction.

Experimentally, the various parameters were determined as follows:  $S$  is obtained from a calibration experiment performed with the dye alone and fixed thereafter for all the experiments. The characteristic diffusion time of the aptamer  $\tau_{D1}$  was obtained from a sample without thrombin. Therefore a single component fit according to equation (6) with  $G_{\text{Diff}}$  from equation (2) was performed. This was repeated with a sample containing a hundredfold excess of thrombin to obtain the characteristic diffusion time of the aptamer thrombin complex  $\tau_{D2}$ . For all the other experiments  $Y$ ,  $\tau_{\text{Tr}}$ ,  $\Theta$  and  $N$  were obtained from individual fits to each sample using equation (6) with  $G_{\text{Diff}}$  from equation (5), while  $\tau_{D1}$  and  $\tau_{D2}$  were fixed. This approach is similar to that by Schürer *et al.* who used FCS to determine the dissociation constant of a moenomycin binding aptamer [13].

### 2.3.2 Experimental setup and methods for FCS measurements

FCS experiments were performed with a commercial FCS setup LSM 510 (Carl Zeiss, Jena, Germany), consisting of the module ConfoCor 2 and an Axiovert 200 microscope equipped with a Zeiss C-Apochromat 403, 40x, NA 1.2 water immersion objective. The 488 nm line of an argon ion laser (Lasos/Zeiss) was used as illumination source for excitation of Oregon Green 488. The laser was operated at the recommended tube current of 6.1 A and the intensity was fixed at 1% to avoid saturation effects. This intensity corresponds to 29.1  $\mu\text{W}$  in the sample volume [14]. Emitted fluorescence was collected at wavelengths exceeding 505 nm after passing the 70  $\mu\text{m}$  pinholes by two avalanche photodiodes. A cross-correlation setup was chosen in all the experiments to suppress the influence of detector afterpulsing. The system was calibrated using a 10 nM solution of Alexa488 dye (Molecular Probes, Invitrogen) in water. The fluorescence signal of this sample was measured ten times for 30 s. The autocorrelation function was calculated for each measurement and fit with equation (1). The parameters  $\tau_{D, \text{Alexa488}} = 23.5 \pm 0.3 \mu\text{s}$ ,  $S = 5.3 \pm 0.2$  and  $N$  are obtained from the fit. The diffusion constant of Alexa488 was determined in reference [14] ( $D = 316 \mu\text{m}^2/\text{s}$ ) using Rhodamine 6G ( $D = 280 \mu\text{m}^2/\text{s}$  [15]) as a reference. Hence, from equation (3) the focal radius is obtained as  $\omega_{xy} = 0.172 \pm 0.002 \mu\text{m}$  (3). The focal volume is  $V = 0.15 \pm 0.01 \text{ fl}$ . Varying amounts of human  $\alpha$ -thrombin (Fluka, Buchs, Switzerland) were added to 25 nM solutions of the aptamer resulting in thrombin concentrations between 2.5 nM and 2.5  $\mu\text{M}$ . The aptamer binding buffer used for the experiments contained 20 mM Tris HCl, 140 mM NaCl, 10 mM  $\text{MgCl}_2$  and 10 mM KCl at pH = 8.5. For each sample the fluorescence signal was measured ten times over 30 s. The collected data was evaluated using the ConfoCor 2 software and fitting procedures. For more detailed error calculations the data was reprocessed using Igor Pro.

### 2.4 Kinetic model for the opening step

For the opening step we have to consider the reactions shown in Figure 1a. In general, in the presence of thrombin a sample of aptamer devices will consist of free aptamers and aptamers bound to the protein (reaction (5)). In addition, the aptamer itself may be present in a folded G quadruplex form or in a random conformation. The equilibrium between these forms is indicated in reaction (1). Fuel strands added to the sample may bind to either species: (2) indicates reaction with an unfolded aptamer strand, (3,4) is the reaction with a folded strand, and (6,7) is the reaction of fuel strand with an aptamer bound to a protein. The latter reactions are subdivided into two steps, where it is assumed that the fuel strand first binds to the unstructured toehold section and then breaks open the rest of the structure. In the following, we use the abbreviations  $x_1 - x_8$  for the concentrations of the molecules

as defined in Figure 1b. The rate equations then read:

$$\begin{aligned}
 \dot{x}_1 &= -k_1x_1 + k_2x_2 - k_3x_1x_3 \\
 \dot{x}_2 &= +k_1x_1 - k_2x_2 - k_5x_2x_3 + k_6x_5 - k_9x_2x_6 + k_{10}x_7 \\
 \dot{x}_3 &= -k_3x_1x_3 - k_5x_2x_3 + k_6x_5 - k_{11}x_3x_7 + k_{12}x_8 \\
 \dot{x}_4 &= +k_3x_1x_3 + k_7x_5 + k_{13}x_8 \\
 \dot{x}_5 &= +k_5x_2x_3 - k_6x_5 - k_7x_5 \\
 \dot{x}_6 &= -k_9x_2x_6 + k_{10}x_7 + k_{13}x_8 \\
 \dot{x}_7 &= +k_9x_2x_6 - k_{10}x_7 - k_{11}x_3x_7 + k_{12}x_8 \\
 \dot{x}_8 &= +k_{11}x_3x_7 - k_{12}x_8 - k_{13}x_8.
 \end{aligned}$$

The backward rates  $k_4 = k_8 = k_{14}$  are already set to zero as the final complex  $x_4$  is assumed to be very stable. Values for the various other rate constants can be estimated as follows: we first focus on the opening of the device in the absence of thrombin, i.e., on reactions (1)–(4). The first reaction is related to the stability of the G quadruplex secondary structure of the aptamer. From thermodynamic data obtained on the quadruplex by Mergny et al. [16], a reaction free energy of  $\Delta G_{298K} = -13.7$  kJ/mol is associated with reaction (1) at  $T = 298$  K and in the presence of  $K^+$  ions which corresponds to an equilibrium constant of  $K \approx 250$ . Under the reaction conditions of our experiments essentially all of the aptamer devices should therefore be in their quadruplex state, rendering reactions (1) and (2) unimportant. Indeed, numerical simulations show that rate constants  $k_1$  and  $k_2$  can be set to zero without changing the final results (see below). Rates  $k_3$ ,  $k_5$  and  $k_{11}$  are expected to be typical DNA hybridization forward rates which are almost always on the order of  $10^{-3}$  nM $^{-1}$  s $^{-1}$  [17] which serves as an initial guess for the numerical treatment. The rate  $k_6$  can be estimated from the typical association and dissociation rate of a 12 bp duplex and its equilibrium constant for hybridization under the given buffer conditions. The equilibrium constant  $K_{\text{toe}} = k_5/k_6$  is calculated to be  $2.46 \times 10^9$  M $^{-1}$  from the Gibbs free energy  $\Delta G_{298K} = -53.5$  kJ/mol which is obtained using the program HYTHER [18]. Thus  $k_6 = 4.1 \times 10^{-4}$  s $^{-1}$ . The rates  $k_9$  and  $k_{10}$  are related to the dissociation constant  $K_d$  of the aptamer device via  $K_d = k_{10}/k_9$ . The dissociation constant is measured by a series of fluorescence correlation spectroscopy experiments where the ratio of initial thrombin to initial aptamer is varied (see Sect. 3).

Two sets of experiments with a different total concentration of aptamer (50 nM and 1  $\mu$ M) and various ratios between protein and aptamer were performed. The initial concentrations for the simulations were chosen accordingly. As will be shown below, the dissociation constant for the device-protein complex was determined to be  $K_d = 122$  nM. From this value we obtain the initial concentration of aptamer devices bound to a protein as:

$$x_7(0) = 1/2[(a + t + K_d) - ((a + t + K_d)^2 - 4at)^{1/2}], \quad (8)$$

where  $a$  and  $t$  are the total aptamer and thrombin concentrations, respectively. The amount of free aptamer then is  $x_2(0) = a - x_7(0)$  while the amount of free thrombin is

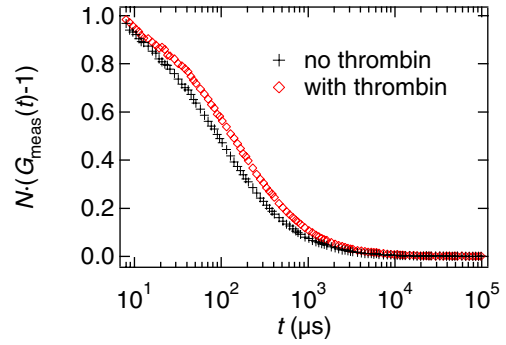


**Fig. 2.** Fluorescence autocorrelation recorded for the aptamer device in the absence and presence of thrombin. The characteristic diffusion times are  $\tau_{D1} = 97.0 \pm 2.6$   $\mu$ s and  $\tau_{D2} = 141.3 \pm 3.5$   $\mu$ s, respectively.

$x_6(0) = t - x_7(0)$ . The fuel strand is added in stoichiometry with the aptamer device  $x_3(0) = a$  and all other concentrations are initially set to zero.

The fluorescence intensity  $I$  measured in FRET experiments is proportional to the concentration of the fluorescent species in the sample, i.e.  $I \propto x_1 + x_2 + x_7 + \xi_1 x_5 + \xi_2 x_8$ . Here it is assumed that binding of the aptamer device to thrombin ( $x_7$ ) does not affect the fluorescence and that binding of fuel strand  $x_3$  to the toehold of the aptamer device ( $x_5$ ) leads to a reduction of the fluorescence by a factor  $0 \leq \xi_1 \leq 1$  due to FRET, whereas binding to the toehold of the thrombin-aptamer complex ( $x_8$ ) leads to a reduction of the fluorescence by a factor  $0 \leq \xi_2 \leq 1$ . As mentioned above, species  $x_1$  does not play an important role in the process considered here and from the simulations described below, we found that  $\xi_1 = 0$  fits the experimental results best. Therefore, the intensity is essentially given by:  $I \propto x_2 + x_7 + \xi_2 x_8$ .

For comparison between experiment and kinetic model, the rate equations were implemented and solved using Matlab (The MathWorks, Natick, MA, USA). To adjust the remaining free rate constants, the least-squares deviation between the experimentally obtained data and the calculated fluorescence intensities was minimized. This was done for all eight experimental time traces simultaneously.

### 3 Results and discussion

In Figure 2, the normalized autocorrelation functions for the aptamer device in the absence of thrombin and in the presence of a hundredfold excess of thrombin is shown. The latter is chosen in order to ensure that all aptamer devices are bound to the protein. From these two curves the characteristic diffusion times are determined by single component fits using equation (6) with  $G_{\text{Diff}}$  from equation (2). For the aptamer alone, a diffusion time of  $\tau_{D1} = 97.0 \pm 2.6$   $\mu$ s is obtained, while for the aptamer bound to thrombin the diffusion time is  $\tau_{D2} = 141.3 \pm 3.5$   $\mu$ s. Hence the diffusion constants are  $D_1 = 76.6 \pm 3.3$   $\mu$ m $^2$ /s and  $D_2 = 52.6 \pm 2.2$   $\mu$ m $^2$ /s. The FCS measurements were

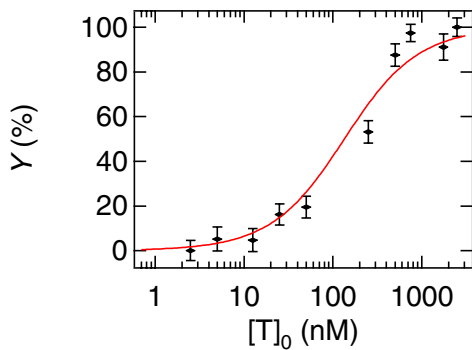


**Fig. 3.** Titration curve obtained from FCS measurements. The percentage of bound aptamer-thrombin-complex ( $Y$ ) is plotted as a function of initial thrombin concentration  $[T]_0$ . The solid line corresponds to a fit of equation (8) to the data with  $K_d$  as the only free parameter. We obtain  $K_d = 122 \pm 16$  nM.

performed at a temperature of  $T = 21.8 \pm 1.0$  °C for which the viscosity of water is  $\eta = 0.96 \pm 0.02$  mPa s [22]. From this the hydrodynamic radii  $R_H = k_B T / 6\pi\eta D$  of the aptamer and the protein-aptamer complex are obtained as  $R_{H1} = 2.9 \pm 0.2$  nm and  $R_{H2} = 4.3 \pm 0.3$  nm. From NMR and X-ray structures, respectively, the size of the aptamer [19] and that of thrombin bound to the aptamer [20] can be estimated. The radius of rotation of these structures is  $r_{\text{Apt}} \approx 1.6$  nm and  $r_{\text{Apt+Th}} \approx 3$  nm. In the aptamer device, the original aptamer structure has been extended by a 12 nt long toehold. In a random conformation this can be expected to have an end-to-end distance of roughly  $\sqrt{2l_p l} = 3.2$  nm, where the contour length is  $l = 12 \cdot 0.43$  nm = 5.2 nm and the persistence length for ssDNA was taken as  $l_p = 1$  nm [21]. Assuming that this length just adds to the diameter of the structures, a radius of rotation of  $r_{\text{Apt-toehold}} \approx 3.2$  nm and  $r_{\text{Apt-toehold+Th}} \approx 4.6$  nm is obtained which is in very good agreement with the hydrodynamic radii.

From FCS measurements with varying thrombin concentrations and two-component fits according to equation (6) with  $G_{\text{Diff}}$  from equation (5), the dissociation constant  $K_d$  of the device-thrombin complex can be obtained. The values displayed in Figure 3 correspond to the value  $Y$  in (5), i.e. the relative amount of aptamer-device bound to thrombin with respect to the initial amount of aptamer-device in solution. The solid line represents a fit with equation (8) (with  $Y = x_7(0)/a$ ) to the data for the given initial concentration of the aptamer device of  $a = 25$  nM. From this fit, a dissociation constant of  $K_d = 122 \pm 16$  nM is obtained. This lies well within the range of dissociation constants previously reported for the unmodified thrombin-aptamer (3 – 450 nM) [4, 23].

Our kinetic model disregards the possibility of dimer formation of thrombin [24, 25] as well as the fact that the aptamer may bind to two distinct binding sites on the protein [20] (see also discussion below). If there were a considerable amount of these structures, they should in fact show up in the FCS experiments as more slowly diffusing species. As this does not seem to be the case in the range

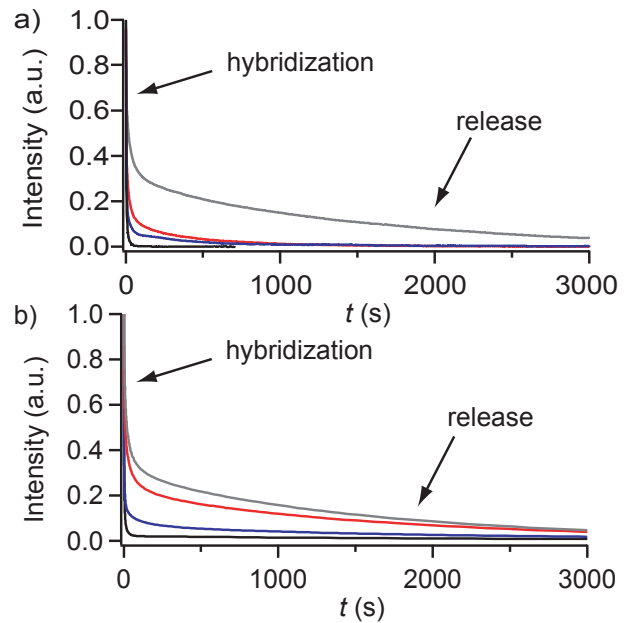


**Fig. 4.** (a) Fluorescence time traces recorded from the aptamer device for a device concentration of  $[A]_0 = 1$   $\mu\text{M}$  and and 5:1, 1:1, 1:5, 0:1 ratios of thrombin to aptamer (from top to bottom) after initiation of the protein release process by the addition of fuel strands. The initial drop corresponds to the hybridization of fuel strand and aptamer device and is second order, whereas the slow decay phase corresponds to the release of protein (see text). (b) Corresponding time traces calculated from the kinetic model for the protein release process using a single set of rate constants for all traces. The overall behavior of the experimental traces is well reproduced. In particular, the fast hybridization and slow release phase correspond well with the experimental data.

of concentrations considered here, we assume that for our kinetic analysis the consideration of simple 1:1 aptamer-thrombin complexes is sufficient.

The experimental results for the fluorescence intensity decay obtained from the aptamer device after addition of the fuel strand are shown in a linear plot in Figure 4a and as semi-log plots in Figure 5 (crosses) for several ratios between device and protein. Figures 4a and 5a contain the traces for  $[A]_0 = x_1(0) + x_2(0) + x_7(0) = 1$   $\mu\text{M}$ , whereas the data points in Figure 5b were recorded for  $[A]_0 = 50$  nM. For both concentrations, when thrombin is added in excess to the aptamer device, the long term decay can be well fit by an exponential as can be immediately seen from the linear slopes in Figure 5. This process corresponds to the release of the protein by the aptamer device. From this exponential, the rate constant  $k_{13}$  can be determined to be  $k_{13} = 6.5 \times 10^{-4}$  s $^{-1}$ . For the numerical simulations,  $k_{13}$  was fixed at that value. In contrast to the behavior at long reaction times, the initial fluorescence drop is quite different for the two sets of time traces in Figures 5a and 5b. This indicates the contribution of a concentration-dependent second order step such as hybridization between fuel and device strand (possibly controlled by rate constants  $k_3, k_5, k_7$  or  $k_{11}$ ). To obtain a

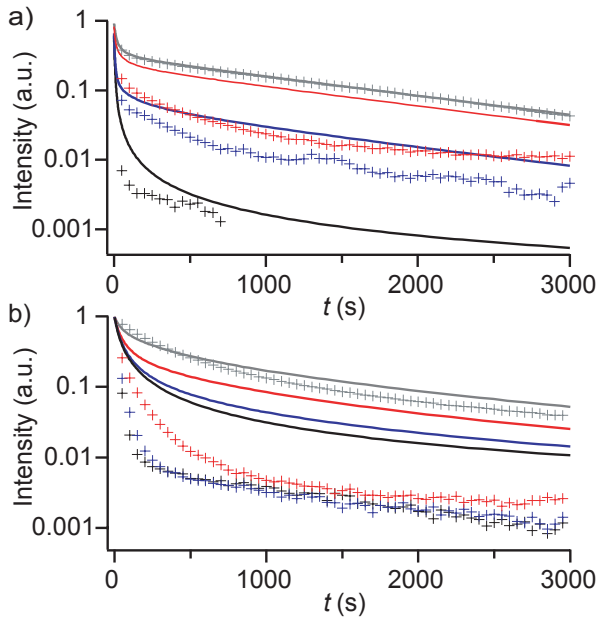


**Fig. 5.** (a) Log-lin plot of the experimental data (one cross for every 50th data point) and the corresponding calculated traces (solid lines) for a device concentration of  $[A]_0 = 1 \mu\text{M}$  and 5:1, 1:1, 1:5, 0:1 ratios of thrombin to aptamer (from top to bottom). This graph combines the traces shown in Figure 4a and 4b in a single plot. (b) Log-lin plot for a device concentration of  $[A]_0 = 50 \text{ nM}$  and 5:1, 1:1, 1:5, 0:1 ratios of thrombin to aptamer (from top to bottom). Comparison to (a) shows that the initial drop which corresponds to the hybridization of fuel strand and aptamer device strongly depends on the DNA concentrations. For the corresponding calculated time traces (solid lines) the same parameters were used as in (a).

quantitative description of the overall process, the kinetic model described above was used to find a set of rate constants which reasonably fits all of the experimental data in Figures 5a and 5b simultaneously. It has to be mentioned that almost perfect agreement between a single time trace and the model can be achieved, as can be seen for the upper trace in Figure 5a. However, we here aimed at a comprehensive description of our data to better capture the concentration dependent processes. Based on the considerations put forward in Section 2.4, rate constants were allowed to vary within physically reasonable boundaries to minimize the least-squares deviation from all of the experimental curves in Figures 5a and 5b at once.

We start the simulations with  $k_3 = k_5 = 10^{-3} \text{ nM}^{-1} \text{ s}^{-1}$ ;  $k_4 = k_8 = k_{14} = 0$ ;  $k_6 = 4.1 \times 10^{-4} \text{ s}^{-1}$ ;  $k_{13} = 6.5 \times 10^{-4} \text{ s}^{-1}$  as fixed parameters and vary the remaining parameters  $k_1, k_2, k_7, k_9, k_{10}, k_{11}, k_{12}, \xi_1$  and  $\xi_2$ .

It turns out that rate constant  $k_1$  can be varied over an extremely wide range and can be even set to zero without deteriorating the result. As  $k_2 \approx k_1/250$  in the model, this essentially makes reactions (1) and (2) unimportant (and, hence,  $k_3$ ). Furthermore, it is found that the best results are obtained if the fluorescence reduction  $\xi_1 = 0$ . This means that in our experiments, reaction (4) is essentially unobservable as it is accompanied only by a neg-

ligible fluorescence change. In summary, in the absence of protein, we essentially observe hybridization of the effector strand with the folded aptamer device as a single reaction step. The rates  $k_6$  and  $k_7$  cannot be resolved in our experiments, and in effect reactions (3) and (4) can be lumped together in one single second order reaction. Instead of  $k_5 = 10^{-3} \text{ nM}^{-1} \text{ s}^{-1}$ ,  $k_6 = 4.1 \times 10^{-4} \text{ s}^{-1}$ , and  $k_7 = 6.7 \times 10^{-4} \text{ s}^{-1}$ , one can use the modified forward rate  $k'_5 = k_5 \cdot k_7 / (k_6 + k_7) = 6.2 \times 10^{-4} \text{ nM}^{-1} \text{ s}^{-1}$  with  $k'_6 = k'_7 = 0$ . The situation is different in the presence of protein. Here reactions (6) and (7) are indeed observed as separate steps.

Of the remaining free kinetic parameters  $k_9, k_{10}, k_{11}, k_{12}$  we find that backward rate  $k_{12}$  again has no significant influence on the result of the numerical simulation. The ratio  $k_{10}/k_9$  is fixed by the dissociation constant  $K_d$  determined above. To find reasonable agreement between simulations and experiment the quenching factor is now set to  $\xi_2 = 0.3$ . Physically, this means that in species  $x_8$  (fuel strand bound to protein-aptamer complex), the distance between the fluorophores is large enough to prevent a complete quenching at this stage. This can be easily understood as a result of the presence of the relatively large protein.

Results of numerical simulations are shown in Figures 4b and 5 (solid lines) for the following parameter settings:  $k_1 = 0, k_2 = 0, k_3 = 0, k_4 = 0, k'_5 = 6.2 \times 10^{-4} \text{ nM}^{-1} \text{ s}^{-1}, k'_6 = 0, k'_7 = 0, k_8 = 0, k_9 = 10^{-5} \text{ nM}^{-1} \text{ s}^{-1}, k_{10} = 1.2 \times 10^{-3} \text{ s}^{-1}, k_{11} = 10^{-4} \text{ nM}^{-1} \text{ s}^{-1}, k_{12} = 0, k_{13} = 6.5 \times 10^{-4} \text{ nM}^{-1} \text{ s}^{-1}, k_{14} = 0, \xi_1 = 0, \xi_2 = 0.3$ . In this context, setting a rate constant to zero means that the corresponding rate cannot be extracted from our experiment, but it may be necessary to choose a non-zero value for different initial concentrations. Compared with the protein-free case, the forward rate  $k_{11}$  for hybridization of the effector strand with the toehold section of the device is reduced by almost one order of magnitude. This indicates that hybridization is indeed slightly inhibited due to the presence of the protein.

There is a good overall agreement between the simulation and the experimental results. The main features, a fast initial drop in fluorescence followed by a slow decay in the presence of thrombin are well reproduced. In Figure 5a, the situation for low and high protein concentrations are particularly well reproduced while there is some deviation for the intermediate case where  $[A]_0 = [T]_0$ . The overall trend is also captured for the lower concentrations (Fig. 5b), and we find the long-term exponential behavior in both calculated and experimental traces. The logarithmic scale exaggerates the deviations at low intensity strengths. However, it becomes clear that the calculated initial decay is slower than that measured for  $[A]_0 = 50 \text{ nM}$ , except for  $[T]_0 = 250 \text{ nM}$  (upper trace), indicating the limitations of our numerical model.

From these results, the following simplistic picture emerges which reasonably accounts for the kinetics of the aptamer device observed experimentally: in the presence of protein, device strands are either bound to the protein

or free in solution. When fuel strands are added, they hybridize to the free device strands in a fast reaction and to the bound device strands in a slightly slower reaction. In the intermediate complex composed of aptamer, protein and fuel strand, the fluorescence is only partly quenched due to FRET. From this intermediate state, the protein is released in a slow first order process and the fuel strand binds to the device strand completely. Obviously the first step — hybridization of fuel and device — is concentration dependent, while the second is not, which explains the main features observed in Figures 4a and 5.

The reduction in hybridization rate between effector strand and toehold in the presence of thrombin is particularly interesting. We can imagine several reasons for the reduced efficiency of hybridization: 1. when thrombin is bound to the aptamer device, the protein simply occupies space and hybridization between toehold and fuel strand might be sterically hindered; 2. the original DNA thrombin aptamer was found to bind to either exosite I or II of thrombin [20]. These exosites — also known as anion-binding exosites — exhibit positively charged residues [26] and may therefore electrostatically interact with the negatively charged backbone of the aptamer. These charged regions can also interact with the toehold of the aptamer device and may therefore reduce its capability for hybridization with the fuel strand. It is well conceivable that in cases where an aptamer binds to less (or more highly) charged residues of a protein, the effect on hybridization efficiency will be quite different.

In addition to the concentration dependence, we also determined the temperature dependence of the release process. Figure 6 shows the intensity decay for  $[A]_0 = 50$  nM and  $[T]_0 = 250$  nM for temperatures  $T = 15$  °C, 20 °C, 25 °C, 30 °C and 35 °C after addition of the fuel strand. As one would expect the fluorescence intensity decreases faster as the temperature rises. However, the influence of temperature on the release process is quite complex as the various chemical equilibria shown in Figure 1 are affected to a different extent. We here concentrate on the kinetic behavior at long times which can be fit well by a single exponential. As discussed above, this corresponds to the protein release process. In the inset of Figure 3, an Arrhenius plot of the release rate constants (corresponding to  $k_{13}$  in Fig. 1) is shown. From a fit of the usual Arrhenius equation  $\ln(k/A) = -E_a/RT$  to the data, we obtain a frequency factor of  $A = 5.3 \pm 1.6$  s $^{-1}$  and an activation energy of  $E_a = 11.7 \pm 0.8$  kJ/mol. Hence,  $E_a$  is on the same order as the energy of a typical hydrogen bond.

## 4 Conclusion

We have studied the kinetics of protein release by a previously introduced aptamer-based molecular device which can be triggered by the addition of a DNA effector strand. The kinetics was studied in FRET experiments for different device concentrations and for various ratios between device strands and protein, and also as a function of temperature. A kinetic model of the relevant reaction steps for

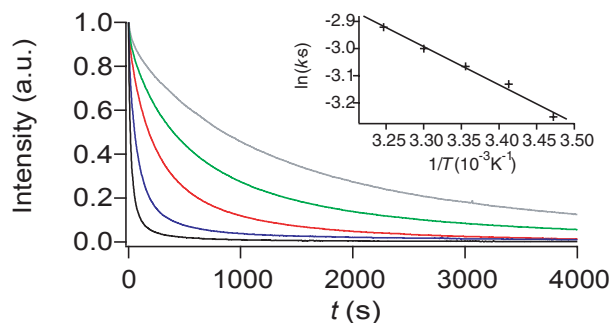


**Fig. 6.** Fluorescence intensity decay for  $[A]_0 = 50$  nM and  $[T]_0 = 250$  nM at temperatures  $T = 15$  °C, 20 °C, 25 °C, 30 °C, and 35 °C (from top trace to bottom trace). In the inset, an Arrhenius plot of the exponential decay rates obtained from the long-time behavior of the fluorescence traces is shown.

the protein release process was developed and compared to the experimentally obtained data in numerical simulations. The results of the calculations suggest a simple two-step mechanism for the protein release, in which the DNA first binds to the “toehold” section of the DNA device, followed by a slow first order protein release process. An important input parameter for the kinetic model — the dissociation constant  $K_d$  of the aptamer-protein complex — was determined in fluorescence correlation spectroscopy experiments to be  $K_d \approx 120$  nM. The hydrodynamic radius obtained for the complex agrees well with structural data from X-ray diffraction and NMR experiments.

Even though our DNA nanodevice is an artificially constructed molecular system with only a few components, already a considerable number of reactions have to be considered to understand its kinetic behavior. As shown in this work, kinetic studies using biophysical techniques such as fluorescence resonance energy transfer and fluorescence correlation spectroscopy supported by numerical modeling can help to elucidate the most relevant kinetic processes governing the device behavior. Such information will become more and more important in the near future, when increasingly complex molecular devices and machines based on DNA will be developed.

We wish to thank Simon Keller and Joachim O. Rädler for introducing us to the FCS technique and letting us use their setup. Continuous support by Jörg P. Kotthaus is also acknowledged. This work has been supported within the Emmy Noether program of the Deutsche Forschungsgemeinschaft (DFG SI 761/2-1/2). W.U.D. acknowledges support by the Alexander von Humboldt foundation.

## References

1. N.C. Seeman, Trends In Biochemical Sciences **30**, 119 (2005)
2. F.C. Simmel, W.U. Dittmer, Small **1**, 284 (2005)
3. W.U. Dittmer, A. Reuter, F.C. Simmel, Angew. Chem. Int. Ed. **43**, 3550 (2004)

4. L.C. Bock, L.C. Griffin, J.A. Latham, E.H. Vermaas, J.J. Toole, *Nature* **355**, 564 (1992)
5. J.R. Lakowicz, *Principles of Fluorescence Spectroscopy*, 2nd edn. (Kluwer Academic, New York, 1999)
6. D. Magde, E. Elson, W.W. Webb, *Phys. Rev. Lett.* **29**, 705 (1972)
7. E.L. Elson, D. Magde, *Biopolymers* **13**, 1 (1974)
8. M. Eigen, R. Rigler, *Proc. Natl. Acad. Sci. USA* **91**, 5740 (1994)
9. J. Widengren, Ü. Mets, R. Rigler, *J. Phys. Chem.* **99**, 13368 (1995)
10. B. Rauer, E. Neumann, J. Widengren, R. Rigler, *Biophys. Chem.* **58**, 3 (1996)
11. P. Schwille, *Cell Biochem. Biophys.* **34**, 383 (2001)
12. O. Krichevsky, G. Bonnet, *Rep. Prog. Phys.* **65**, 251 (2002)
13. H. Schürer, A. Buchynskyy, K. Korn, M. Famulok, P. Welzel, U. Hahn, *Biol. Chem.* **382**, 479 (2001)
14. T. Liedl, S. Keller, F.C. Simmel, J.O. Rädler, W.J. Parak, *Small* **1**, 997 (2005)
15. D. Magde, E.L. Elson, W.W. Webb, *Biopolymers* **13**, 29 (1974)
16. J.L. Mergny, A.T. Phan, L. Lacroix, *FEBS Lett.* **435**, 74 (1998)
17. V.A. Bloomfield, D.M. Crothers, I. Tinoco, Jr, *Nucleic Acids* (University Science Books, Sausalito, 2000), p. 291
18. N. Peyret, J. SantaLucia, HYTHER, version 1.0, Wayne State University
19. P. Schultze, R.F. Macaya, J. Feigon, *J. Mol. Biol.* **235**, 1532 (1994)
20. K. Padmanabhan, K.P. Padmanabhan, J.D. Ferrara, J.E. Sadler, A. Tulinsky, *J. Biol. Chem.* **268**, 17651 (1993)
21. B. Tinland, A. Pluen, J. Sturm, G. Weill, *Macromolecules* **30**, 5763 (1997)
22. D.R. Lide, H.V. Kehiaian, *CRC Handbook of Thermophysical and Thermochemical Data* (CRC Press, Boca Raton, 1994)
23. J.W.J. Li, X.H. Fang, W.H. Tan, *Biochem. Biophys. Res. Comm.* **292**, 31 (2002)
24. P.J. Anderson, *Biochem. J.* **336**, 631 (1998)
25. Y. Liu, C. Lin, H. Li, H. Yan, *Angew. Chem. Int. Ed.* **44**, 4333 (2005)
26. J.A. Huntington, *J. Thromb. Haemost.* **3**, 1861 (2005)